atmosphere

MDPI

Article

Lidar Complex for Control of the Ozonosphere over Tomsk, Russia

Alexey A. Nevzorov [1,*], Alexey V. Nevzorov [2], Olga Kharchenko [2] and Yaroslav O. Romanovskii [1]

[1] Laboratory for Remote Sensing of the Environment, V.E. Zuev Institute of Atmospheric Optics SB RAS, 634055 Tomsk, Russia; romanovskii.io17@physics.msu.ru
[2] Center of Laser Atmosphere Sensing, V.E. Zuev Institute of Atmospheric Optics SB RAS, 634055 Tomsk, Russia; nevzorov@iao.ru (A.V.N.); olya@iao.ru (O.K.)
* Correspondence: naa@iao.ru; Tel.: +7-382-249-0462

Abstract: We present a union of three measurement systems on the basis of the Siberian lidar station and mobile ozone lidar. The lidars are designed for studying the ozonosphere using the method of differential absorption and scattering, as well as for studying aerosol fields using elastic single scattering. The systems are constructed on the basis of Nd:YAG lasers (SOLAR) and an Nd:YAG laser (LOTIS TII), a XeCl laser (Lambda Physik) and receiving telescopes assembled using the Kassegrain system with a diameter 0.35 m and the Newtonian 0.5 m system. Lidars operate in photon-counting mode and record lidar signals with a spatial resolution from 1.5 m to 160 m at sensing wavelengths of 299/341 nm in the altitude range of ~0.1–12 km and ~5–20, and at 308/353 nm in the altitude range of ~15–45 km. The union of these three measurement systems was used to carry out field experiments of atmospheric lidar sensing in Tomsk and to present the results of retrieving the vertical profile of the ozone concentration. In this study, coverage of the entire ozonosphere by the lidars was carried out for the first time in Russia.

Keywords: atmosphere; lidar sensing; lidars; ozone

Citation: Nevzorov, A.A.; Nevzorov, A.V.; Kharchenko, O.; Romanovskii, Y.O. Lidar Complex for Control of the Ozonosphere over Tomsk, Russia. *Atmosphere* **2024**, *15*, 622. https://doi.org/10.3390/atmos15060622

Academic Editor: David F. Plusquellic

Received: 9 April 2024
Revised: 9 May 2024
Accepted: 16 May 2024
Published: 22 May 2024

1. Introduction

The minor atmospheric gases, among which are water vapor, carbon dioxide, ozone, nitrogen and sulfur oxides, carbon monoxide, and many others, are optically active components of the atmosphere that exert a strong effect on the following processes: weather formation, pollution of the water basin by industrial emissions, conversion of solar radiation, and the propagation of optical waves [1]. Greenhouse gases, especially ozone and the gas components of ozone cycles, clouds, and aerosol fields are the main climate-forming factors from the viewpoint of the radiation balance of the atmosphere [1]. About 85% of ozone resides at altitudes within the stratosphere, from 15 to 45 km; it generated from molecular oxygen through the attachment of atomic oxygen to its molecules under the influence of ultraviolet solar radiation. There are a number of methods that can be used to study this gas, and a special role is played by the method of differential absorption [2,3], showing the necessary sensitivity for studying the concentrations of gas components in the free atmosphere. Lidar studies of the ozone vertical distribution (OVD) are practically the only inexpensive and exact tool in permanent use to acquire information about the state of the ozonosphere [1]. The considerable advantages of laser sensing should be considered, such as the high spatiotemporal resolution of the lidar data obtained. At the Siberian Lidar Station (SLS) at the V.E. Zuev Institute of Atmospheric Optics, Siberian Branch, Russian Academy of Sciences, we have created and successfully operated unique lidars, which are listed in the "Set of unique experimental installations of national significance" according to government regulations [4]. The SLS researchers perform regular measurements, making it possible to control the dynamics of OVD over Tomsk in the upper troposphere/stratosphere (~5–45 km). Based on the experience accumulated during the servicing and modernization

of the SLS measurement complex, in 2021 we developed and put into operation a mobile lidar with the sensing wavelengths of 299 and 341 nm [5]. The measurements carried out by this lidar cover the altitudes from 0.1 to 12 km and complement the SLS studies in the altitude range of ~0.1–5 km.

At large spatial scales and in relatively short periods of time, the ozone vertical distributions (OVDs) can be obtained using operational lidar stations that are located worldwide, such as the NDACC (Network for the Detection of Atmospheric Composition Change) [6]. Separately, we should note the existence of lidar systems on mobile platforms, such as TOLNet (Tropospheric Ozone Lidar Network) [7], which generally operate in a united group in the framework of research campaigns. The successful use of lidars makes it possible to carry out intercalibration works on satellite instruments when a comparison cannot be made against the reference (ozonesonde) for validation.

Currently, there are lidar stations operating worldwide that cover both the stratosphere–troposphere and the near-surface layer. Here, we will list a small number of lidars that are located in different parts of the globe: the Arctic Stratospheric Observatory (AStrO), Canada [8]; Athens, Greece [9]; Beijing, China [10,11]; Eureka, Canada [12]; Goddard Space Flight Center (GSFC), United States [13,14]; Héféi, China [15,16]; Lauder, New Zealand [17]; Mauna-Loa (MLO), Hawaii, United States [18]; Maïdo Observatory, Reunion Island, France [19,20]; Observatoire de Haute Provence (OHP), France [21,22]; Tsukuba, Japan [23,24]; Troitsk, Russia [25]; the Table Mountain Facility (TMF), United States [26,27]; SLS or Tomsk, Russia [5,28]; Vladivostok, Russia [29]; and the Yangbajing Observatory, China [30]. All of these lidar systems, presented in Table 1, use stimulated Raman scattering (SRS) cells to obtain information-bearing wavelengths for ozone sensing.

Table 1. Main lidar characteristics.

Station or City	Laser	Pumping Wavelength, nm	SRS	Wavelength Pairs, nm	Altitude Range, km	Error, %	Mirror, m	Coordinates
AStrO [8]	XeCl	308	H_2	308/353	10–35	5–30	1	80° N, 86° W
Athens [9]	Nd:YAG	266	D_2	266/289 289/299 289/316	0.5–2.7	10 35 65	0.25	37.97° N, 23.71° E
Beijing [10,11]	Nd:YAG XeCl Nd:YAG	266 308 355	D_2 H_2 -	289/299 308/355	0.15–3 10–35	10 5–30	0.4 0.2	39.90° N, 116.39° E
Eureka [12]	Nd:YAG	266	CO_2	276/287 287/299	0.5–1.8 0.5–3.5	10	0.2	80° N, 86° W
GSFC [13,14]	Nd:YAG XeCl Nd:YAG	266 308 355	D_2 H_2 –	289/299 308/355	1.5–12 10–50	16–19 5–30	0.45 0.76	37.1° N, 76.39° W
Héféi [15,16]	Nd:YAG XeCl	266 308	H_2 D_2 CH_4	308/353 299/288 289/308	18–40 0.5–2 4–18	5–30 10 25	0.3 0.62	31.82° N, 117.22° E
Lauder [17]	XeCl	308	H_2	308/353	10–48	5–30	0.6	45.0° S, 169.7° E
MLO [18]	XeCl Nd:YAG	308 355	H_2 -	308/353	15–55	5–30	1	19.5° N, 155.6° W
Maïdo [19,20]	Nd:YAG XeCl Nd:YAG	266 308 355	D_2 - -	289/316 308/355	6–17 15–45	20 5–30	4 units 0.5	21° N, 55° E
OHP [21,22]	Nd:YAG XeCl Nd:YAG	266 308 355	D_2 –	289/316 308/355	3–14 15–45	10 5–20	0.4 4 units 0.53	43.94° N, 5.71° E

Table 1. *Cont.*

Station or City	Laser	Pumping Wavelength, nm	SRS	Wavelength Pairs, nm	Altitude Range, km	Error, %	Mirror, m	Coordinates
Tsukuba [23,24]	Nd:YAG XeCl Nd:YAG XeF	266 308 355 351	CO_2 D_2	276/287 287/299 308/355 308/351 308/339	0.4–3 3–10 15–45 10–45 10–45	3–9 5–30	0.25 0.6 1 1 2	36.05° N, 140.13° E
Troitsk [25]	KrF XeCl	248 308	H_2 D_2	277/308 292/308	0.5–4.5 4–10	15 30	0.6	54.09° N, 61.57° E
TMF [26,27]	Nd:YAG XeCl Nd:YAG	266 308 355	D_2 H_2 H_2	289/299 308/353	3–18 15–50	7–14 5–30	0.91 0.9	34.4° N, 117.7° W
SLS [5,28]	Nd:YAG Nd:YAG XeCl	266 266 308	H_2 H_2 H_2	299/341 299/341 308/353	0.1–12 5–20 15–45	8–22 6–18 5–35	0.35 0.5	56.50° N, 85.00° E
Vladivostok [29]	XeCl	308	H_2	308/353/331	5–40	2–30	0.6	43.3° N, 132° E
Yangbajing [30]	Nd:YAG XeCl	266 308	D_2 H_2	289/299 308/355	5–10 8–19 19–32 32–50	<30 <30 <30 >30	4 units 1.25 4 units 0.21 1	30°5′ N, 90°33′ E

As can be seen from Table 1, these lidar have, as constituent parts, both excimer lasers, which are usually used for sensing at stratospheric altitudes, and solid-state generators of coherent radiation for coverage of the troposphere. Not all of the above-listed lidar systems, except the SLS, can cover the entire ozonosphere. This competitive advantage of the SLS made it possible to comprehensively study the processes occurring in the entire ozone layer.

The purpose of this paper is to present the Russia-unique union of three measurement systems on the basis of the Siberian Lidar Station and mobile lidar, capable of covering the ozonosphere over Tomsk in the altitude range of 0.1–45 km.

2. Method of Differential Absorption and Scattering

There are a few methods for studying and detecting atmospheric ozone, among which, a special place is occupied by the method of remote detection and identification using the selective absorption of laser radiation, which has maximum sensitivity when probing gas over long distances (differential absorption and scattering lidar method or DIAL method). The DIAL method uses a comparison of received lidar signals at the ozone absorption wavelength and a reference wavelength. Analysis of the ratio of the two lidar signals at the sensing wavelengths makes it possible to estimate the ozone's spatial distribution.

To retrieve the gas concentration $n(Z)$ in the atmosphere, we use the following formula [3]:

$$n(Z) = \frac{1}{2\left[k_{on}(Z,T) - k_{off}(Z,T)\right]} \times \left\{ \frac{d}{dZ} ln\left[\frac{N_{off}(Z)}{N_{on}(Z)}\right] - C(Z) \right\} \quad (1)$$

where $k_{on}(Z,T)$ and $k_{off}(Z,T)$ are the differential absorption cross sections, which depend on the temperature T [31,32] at the corresponding sensing wavelengths λ_{on} and λ_{off}, $N_{on}(Z)$ and $N_{off}(Z)$ are recorded lidar signals at the wavelengths λ_{on} and λ_{off} at the altitude H along the sensing path, λ_{on} is the wavelength of the line of the laser radiation near the center of the gas absorption line, λ_{off} is at the wing of absorption line, and $C(Z)$ is aerosol correction.

Based on the method of differential absorption and scattering, or the DIAL method, the inverse problem is solved, and the vertical profile of ozone concentration is retrieved. As is known, at tropospheric altitudes the aerosol filling factor is high. Therefore, to increase the reliability of the reconstructed profiles, we apply aerosol correction. A similar example was examined in detail in [33], where it was shown that, without aerosol correction, the profiles overestimate the ozone concentration in the troposphere.

It is important to know the vertical distribution of the retrieval error to check the ozone profiles obtained and to carry out intercalibration tests with data from different sources of OVD measurements. The error within OVD retrieval from lidar measurements is calculated using the following formula:

$$E_{sum}^2 = e_1^2 + e_2^2 + e_3^2 + e_4^2, \quad (2)$$

where e_1 is the absorption cross section error, e_2 is the root mean square error (RMSE) in the lidar measurements in the photon counting mode, e_3 is the error in retrieving the scattering coefficient, and e_4 is the error within the temperature profile.

The cross-section error was obtained from works [31,32] and corresponds to ~3%. The temperature profile error is usually taken from MetOp meteorological satellite observations, in which it is generally within ~2% [34].

The RMSE of lidar measurements is [7]:

$$e_2^2 = 0.25 \times \left[\frac{1}{N_{on}(Z) - N_{noise}(Z)} + \frac{1}{N_{off}(Z) - N_{noise}(Z)} \right], \quad (3)$$

where $N_{noise}(Z)$ is the background value, obtained from lidar measurements.

The formula for the error of retrieving the scattering coefficient has the form

$$e_3^2 = \frac{N_{off}(Z)}{\left[N_{off}(Z) - N_{noise}(Z) \right]^2} + \frac{N_{off}(Z_{calib})}{\left[N_{off}(H) - N_{noise}(Z_{calib}) \right]^2} + K, \quad (4)$$

where Z_{calib} is the calibration altitude, and K is a value arising from assumptions in the method of obtaining the scattering coefficient and is 3×10^{-4} [35].

3. Lidar Systems

To carry out continuous monitoring of the ozonosphere in the altitude range of ~5 km to ~45 km at sounding wavelengths of 299/341 nm and 308/353 nm, the SLS lidars must be in readiness mode [28]. Lidars allow the stratosphere and troposphere around the tropopause region to be controlled. This makes it possible to record seasonal variations in the ozonosphere and processes of tropospheric–stratospheric exchange, as well as factors that influence the planet's climate (such as traces of volcanic eruptions). Figure 1 presents a block diagram of the SLS lidar for sensing of ozone in the upper troposphere–stratosphere.

As can be seen from Figure 1, the SLS lidar complex uses one telescope and two pulsed lasers (excimer XeCl and Nd:YAG lasers), and depending on the sensing goal, i.e., either stratospheric (308/353 nm) or tropospheric ozone (299/341 nm), the experimenter can install the spectral optics into the spectral selection cell.

To study the troposphere, the Nd:YAG laser (LOTIS TII LS–2134UT) is turned on. Nd:YAG laser radiation (266 nm) passes through a lens, which focuses the radiation towards the center of the SRS cell. The pumping power density required to obtain the SRS effect is provided by a lens with a focal length of 0.52 m. The pumping pulse energy at a wavelength of 266 nm reaches 25 mJ. Lenses are installed in place of the input and output windows in the SRS cell. The SRS cell is a stainless-steel pipe with diameter of 3 cm and a length of 1.04 m, in which a constant pressure of hydrogen 2 atm is maintained. At the output of the SRS cell, laser radiation passes through a collimating lens with a focal length of 0.52 m. The lenses are made of KU-1. Next, laser radiation with wavelengths of

299 and 341 nm is directed into the atmosphere through the output mirror. The output mirror alignment unit is designed on the basis of stepper motors with the ability to be controlled by a computer, with the computer sending commands to the stepper motors through the cable connecting them.

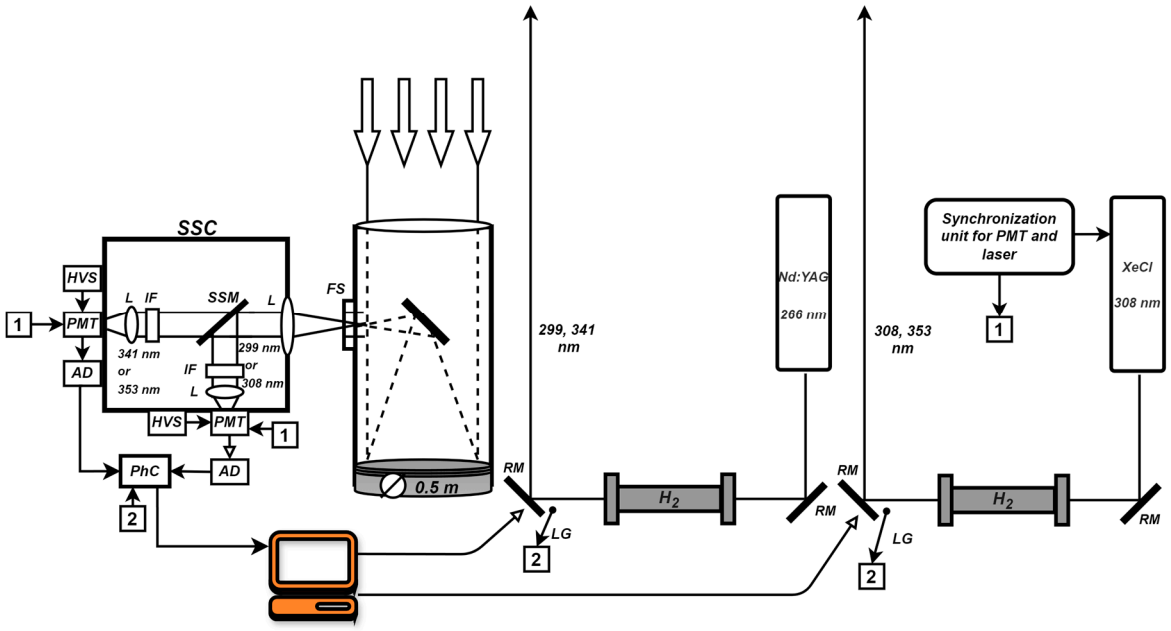

Figure 1. Block diagram of ozone lidar: 1 is the signal for controlling the photomultiplier (PMT) blocks; Nd:YAG and XeCl are the laser sources; L are lenses; H_2 is the hydrogen-filled SRS cell; RM are rotating mirrors; FS is the field stop; SSC is the spectral selection cell with PMT; SSM is the spectral splitting mirror; IF is the interference filters; AD are amplifiers–discriminators; HVS are high voltage supplies; PhC is PHcount6/2 photon counter; LG or 2 is light guide for launching photon counter; Computer is personal computer for data acquisition and storage, controlling the angle of RM.

In cases where it is necessary to conduct lidar sensing in the stratosphere, the XeCl laser (Lambda Physik LPX 220i) is launched. This uses XeCl laser radiation (308 nm) focused through an SRS cell with hydrogen, and is equipped with focusing and collimating lenses (lens focal length 0.77 m, material KU-1) in place of the input and output windows. The pumping pulse energy at a wavelength of 308 nm reaches 200 mJ. The SRS cell is a stainless-steel pipe with a diameter of 3 cm and a length of 1.54 m, in which a constant pressure of 10 atm is maintained. Next, laser radiation with wavelengths of 308 and 353 nm is directed through the output mirror into the atmosphere through the output mirror adjustment unit.

The backscattered optical lidar signal from the atmosphere is collected by a receiving antenna designed according to the Newtonian scheme with a main receiving mirror of 0.5 m in diameter with a focal length of 1.5 m. The field diaphragm is located at the focus of the Newtonian telescope. After the field diaphragm with a diameter of 2.5 mm, the optical signal enters the spectral selection cell and is recorded by PMTs. Electrical signals from the R7207-01 photomultiplier are amplified by C3866 discriminator amplifiers from HAMAMATSU. The PMT and the C3866 discriminator amplifiers are connected to each other by an electrical signal transmission cable. High-voltage power supplies, bolted to the outer casing of the cell, power the PMT through high-voltage wires. Amplified electrical signals are sent from the C3866 discriminator amplifiers through electrical signal transmission cables to the «PHCOUNT 6/2» photon counter in the lidar recording path, where the counter sums the digitized signals over 2048 time intervals with a maximum resolution of 66.66 ns (10 m). All devices and the «PHCOUNT 6/2» counter are screwed

onto the optical bench. The photon counter is connected to the computer through a USB cable through which the digital lidar signals are transmitted.

The mobile lidar is designed to cover the altitudes that are not covered by the SLS lidar complex and to study the specific features of the OVD in the altitude range of ~0.1–12 km, as well as to trace the seasonal variations, and to study how the processes of stratosphere–troposphere exchange close to the near-ground layer act on the mobile lidar with sensing wavelengths of 299 nm and 341 nm [5]. This mobile lidar is the only one in Russia.

Figure 2 presents a block diagram of the mobile lidar.

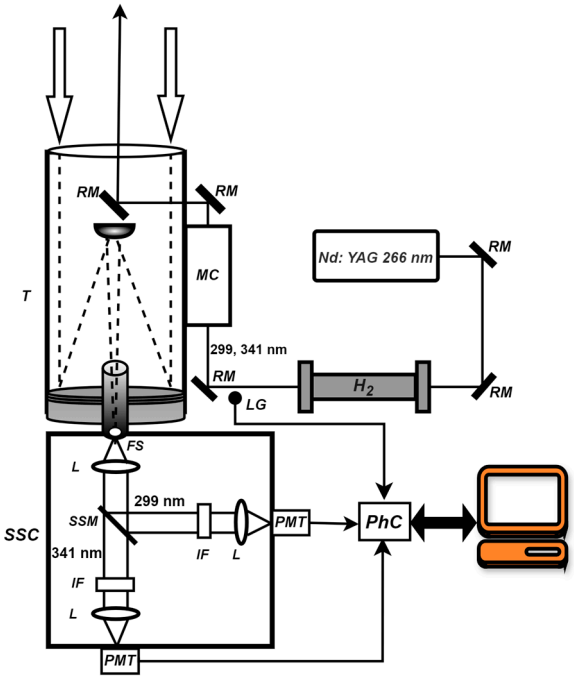

Figure 2. Block diagram of the mobile ozone lidar: Nd:YAG is the solid-state laser; RMs are rotating mirrors; H_2 is the hydrogen-filled SRS cell, equipped with lenses; MC is a mirror collimator; T is receiving telescope, assembled according to Kassegrain scheme with the 0.35 m diameter main mirror; SSC is the spectral selection cell; FS is the field stop; Ls are lenses; SSM is the spectral splitting mirror; IFs are interference filters; PMTs are modules of H12386-210 HAMAMATSU photomultiplier tubes; PhC is PHCOUNT_4E photon counter; LG is light guide for launching photon counter; Computer is personal computer for data acquisition and storage.

The mobile lidar works in the following way. Under the condition of a cloudless sky at night, the Nd:YAG laser (Solar Laser System QX 500) is launched. The QX 500 generates 266 nm wavelengths (fourth harmonic). Rotating mirrors direct the laser radiation to the SRS cell which contains hydrogen under a pressure of 2 atm. Lenses made of KU-1 material with a focal length of 0.52 m are installed at the input and output of the cell. They provide the necessary pumping power density to obtain the effect of SRS conversion of the fourth harmonic to wavelengths sensing at 299 nm and 341 nm. The SRS cell is made of a stainless-steel pipe with an internal diameter of 3 cm and a length of 1.04 m. The laser radiation input into the SRS cell reaches 25 mJ. At the exit from the SRS cell, the radiation, reflected from the adjustable rotating mirror, enters the mirror collimator, which expands the beam five times. This makes it possible to reduce the radiation divergence to 0.2 mrad. The mirror collimator directs radiation to the output mirror located behind the counter mirror of the Cassegrain telescope with a main mirror diameter of 0.35 m and a focal length of 0.7 m. Due to the size of the counter mirror, the telescope has a dead zone of about 100 m, within which the lidar system is not capable of receiving signals. Backscattered laser radiation received by the telescope from the atmosphere passes through a field diaphragm with a diameter of 1 mm, which is installed at the focus of the main receiving mirror. After

passing through the field diaphragm, the optical signal enters the collimating lens. After the lens, the radiation penetrates into the spectral selection cell. In the cell, a dichroic mirror reflects radiation with a wavelength of 299 nm and transmits radiation with wavelength of 341 nm. Afterwards, the skeletonized radiation passes through narrow-band interference filters and is focused by lenses onto the photocathodes of the HAMAMATSU H12386-210 photomultiplier modules. Using PMT modules, the father signal is converted into electrical signal of transistor–transistor logic (TTL) levels. The PMT modules are connected by coaxial cables to the autonomous photon counter «PHCOUNT_4E». The counter summarizes the digitized signals over 16384 time intervals with a resolution of 10 ns (1.5 m). Typically, PHCOUT_4E is connected to a computer through Wi-Fi. The optical fiber installed after the SRS cell is used to synchronize the operation of the photon counter with the pulsed Nd:YAG laser.

The main technical characteristics of the union of the three lidars are presented in Table 2.

Table 2. Main technical characteristics of lidars.

	Mobile Lidar	**SLS Lidar Complex**	
Transmitter	SOLAR QX 500	LOTIS TII	LPX–120i
Wavelength of laser radiation, λ nm	266	266	308
Cooling system	Air-cooled	Water-cooled	Water-cooled
Energy per pulse, mJ (corresponds to λ)	up to 25	up to 25	up to 200
Pressure in hydrogen-filled stimulated Raman scattering cell, atm	2	2	10
Sensing wavelengths, λ nm	299/341	299/341	308/353
Pulse repetition rate, Hz (corresponds to λ)	20/20	15/15	100/100
Pulse duration, ns	10	5–6	25–27
Mirror collimator	Five-fold (×5)	-	-
Divergence, mrad	0.2	0.5	2.5
Receiver	Kassegrain telescope	Newtonian telescope	
Mirror diameter, m	0.35	0.5	
Focal distance, m	0.7	1.5	
Photon counter	PHCOUNT_4E	PHcount6/2	
Receiving channels, items	4	2	
Channels for recording overflow, items	4	-	
Counting rate, MHz per channel	200	200	
Input impedance, Ohm	50	50	
Synchronization	Transistor Transistor Logic (TTL) signal with the frequency up to 10 kHz, or optical signal	Optical signal	
Spatial resolution, m	1.5–150	10–160	
Interface of communication with computer	Ethernet, Wi-Fi	Ethernet	
Altitude range, km	~0.1–12	5–20	15–45
Hamamatsu PMT	H12386-210, 2 items	R7207-01, 2 items	

4. Discussion

The measurements of stratospheric ozone using the SLS lidar complex with the spatial resolution of 50 m last for ~30–40 min. Then, the optics of the spectral selection cell are changed in 5 min to receive backscattered radiation from the atmosphere at another wavelength pair. The ozone measurements at 299/341 nm with a spatial resolution of 10 m last for ~40 min. The beginning of the mobile lidar sensing the troposphere coincides with the start of the SLS lidar complex's measurements after its rearrangement to receive sensing wavelengths of 299/341 nm. A single file from the mobile lidar with the spatial resolution of 1.5 m is saved for 5 min.

A number of field measurements of ozonosphere over Tomsk were carried out on clear-sky nights with the spatial resolution of 50 m. The experimental data were used to solve the inverse problem and to retrieve the ozone profiles. By solving the inverse problem based on Equation (1), we retrieved the ozone profiles. The results of using the union of three lidar systems for sensing the ozonosphere in the form of the ozone profile with the retrieval error and Aura and MetOp data [36,37] are presented in Figure 3.

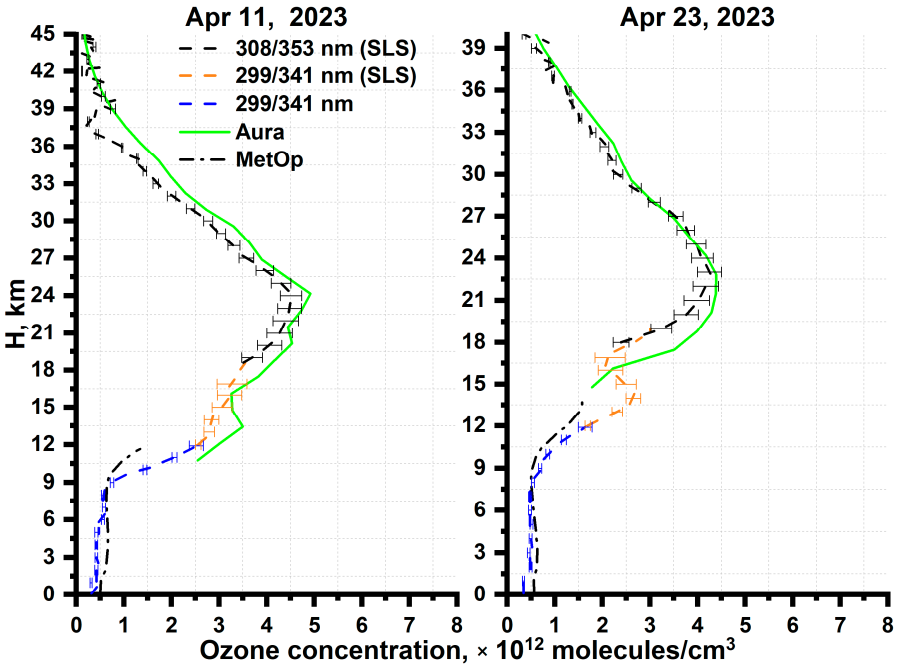

Figure 3. Retrieved ozone profiles.

As is known, the nature of stratospheric ozone is more static on larger horizontal and vertical spatial scales than the vertical distribution of tropospheric ozone. Therefore, successive lidar measurements tend to be in good agreement in the stratosphere. This control problem in our case is solved by a lidar with wavelengths of 308/353 nm, which covers altitudes from ~15 km to ~45 km. From the profiles shown in Figure 3, it is clear that the tropopause is located at approximately 9 km. Therefore, in order to cover the altitude range of the upper troposphere–lower stratosphere, which is ~5–20 km (Figure 3 shows the example of 12–20 km), a stationary lidar was used, operating at a pair of wavelengths of 299/341 nm and a lidar signal accumulation time of ~40 min. This factor contributes to the standard error, which is confirmed by the data in Figure 4. Therefore, mobile and stationary lidar data at the wavelength pair of 299/341 nm in the altitude range of 9–12 km are usually very close and are included in the error corridor because they cover the lower stratosphere. Finally, in lidar sensing experiments, due to the dynamic nature of the tropospheric ozone (0.1–9 km), a short period for the registration of lidar signals is used and because of this factor we believe that short-term measurements from a mobile lidar are more reliable than data from stationary measurements (5–9 km).

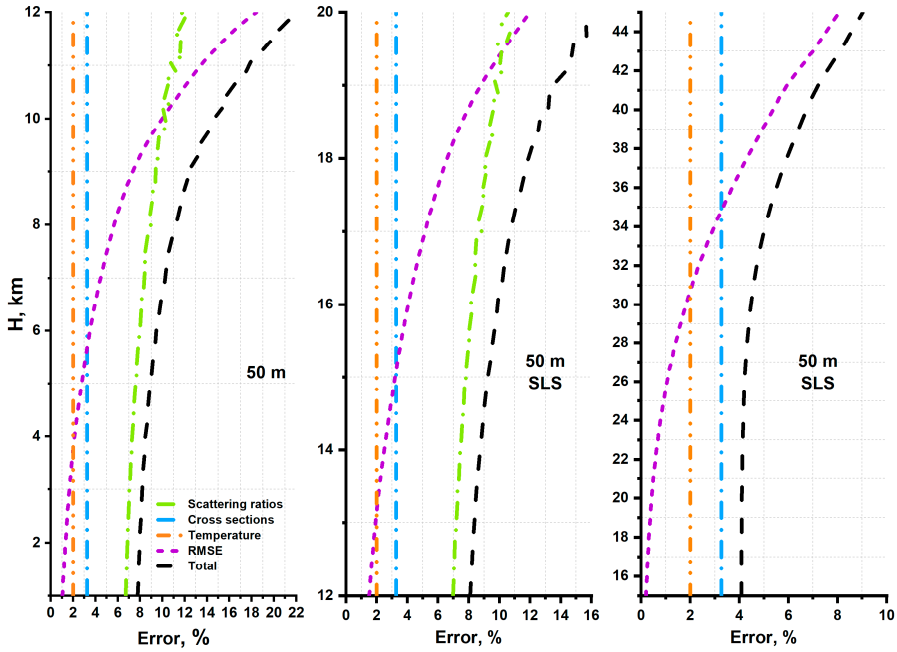

Figure 4. Retrieval error.

Using Equation (2), Figure 4 presents the vertical error distribution of retrieving data with the spatial resolution of lidar signals of 50 m.

As can be seen from Figure 4, the total error increases from 7. 8% at 0.1 km to 22% at 12 km; it is 8.1–17% in the altitude range of 12–20 km, and 4.1–9% in the altitude range of 16–45 km. Evidently, this profile, covering the altitudes from the near-ground layer to the tropopause, shows a large amount of error compared to other profiles, primarily because of the effect of the retrieval error of the scattering ratio and standard deviation.

5. Conclusions

To solve the problem of controlling the ozonosphere in the altitude range from ~0.1 km to ~45 km, we united three lidar systems into a single lidar complex on the basis of the SLS and a mobile lidar; this union allowed us to obtain lidar signals with a spatial resolution from 1.5 m to 160 m. The retrieval error increased from ~4% to 22% at the spatial resolution of lidar signals of 50 m. This lidar complex for ozone measurements is a unique solution to the problem of controlling the ozonosphere in the Russian Federation. The field experiments confirm that the union is efficient. Due to this combination of three ozone lidar systems, it is possible to monitor stratospheric ozone, which carries information about global processes affecting the planet's climate. These are, of course, the strongest volcanic eruptions. The processes occurring in the troposphere are local in nature and are observed by mobile and stationary lidars (299/341 nm). The union of these lidar systems makes it possible to connect the global processes of ozonosphere variability in the stratosphere with processes of local variability in the troposphere; namely, it can be used to assess stratospheric–tropospheric exchange and can be a source of information about these phenomena for instruments that monitor the surface layer of the atmosphere. Lidars can provide high spatial resolution data, which will be useful for comparing ozone measurements with satellite instruments. In the future, we have plans to further develop the presented combination of lidar systems. The mobile lidar will be modified to have a four-channel mode for recording lidar signals, which will increase the altitude range of ozone measurements to ~18 km.

Author Contributions: Conceptualization, A.V.N., A.A.N., Y.O.R. and O.K.; methodology, A.V.N. and A.A.N.; validation, A.A.N. and A.V.N.; formal analysis, A.A.N.; resources, A.V.N. and A.A.N.; data curation, A.V.N. and A.A.N.; writing—original draft preparation, A.A.N.; writing—review and editing, A.A.N.; visualization, A.A.N.; supervision, A.A.N.; project administration, Y.O.R. and A.A.N. All authors have read and agreed to the published version of the manuscript.

Funding: This work was supported by the Russian Science Foundation (no. 21-79-10051), https://rscf.ru/project/21-79-10051/ (accessed on 13 May 2024).

Institutional Review Board Statement: Not applicable.

Informed Consent Statement: Not applicable.

Data Availability Statement: The data presented in this study are available on request from the corresponding author.

Conflicts of Interest: The authors declare no conflicts of interest.

References

1. Belan, B.D. Tropospheric ozone. 1. Properties and role in natural and anthropogenic processes. *Atmos. Ocean. Opt.* **2008**, *21*, 262–280.
2. Belan, B.D. Tropospheric ozone. 2. Measurement instrumentation. *Atmos. Ocean. Opt.* **2008**, *21*, 345–368.
3. Measures, R.M. *Laser Remote Sensing. Fundamentals and Applications*; Reprint 1984; Krieger Publishing Company: Malabar, FL, USA, 1992; pp. 237–280.
4. Siberian Lidar Station. Available online: http://ckp-rf.ru/usu/73575/ (accessed on 9 April 2024).
5. Nevzorov, A.A.; Nevzorov, A.V.; Kravtsova, N.S.; Kharchenko, O.V.; Romanovskii, Y.O. Mobile Lidar for Sensing Tropospheric Ozone. *Atmos. Ocean. Opt.* **2023**, *36*, 562–568. [CrossRef]
6. De Mazière, M.; Thompson, A.M.; Kurylo, M.J.; Wild, J.D.; Bernhard, G.; Blumenstock, T.; Braathen, G.O.; Hannigan, J.W.; Lambert, J.-C.; Leblanc, T.; et al. The Network for the Detection of Atmospheric Composition Change (NDACC): History, status and perspectives. *Atmos. Chem. Phys.* **2017**, *18*, 4935–4964. [CrossRef]
7. Leblanc, T.; Brewer, M.A.; Wang, P.S.; Granados-Muñoz, M.J.; Strawbridge, K.B.; Travis, M.; Firanski, B.; Sullivan, J.T.; McGee, T.J.; Sumnicht, G.K.; et al. Validation of the TOLNet lidars: The Southern California Ozone Observation Project (SCOOP). *Atmos. Meas. Tech.* **2018**, *11*, 6137–6162. [CrossRef]
8. Carswell, A.I.; Pal, S.R.; Steinbrecht, W.; Whiteway, J.A.; Ulitsky, A.; Wang, T.Y. Lidar measurements of the middle atmosphere. *Can. J. Phys.* **1991**, *69*, 1076–1086. [CrossRef] [PubMed]
9. Mytilinaios, M.; Papayannis, A.; Tsaknakis, G. Lower-free tropospheric ozone DIAL measurements over Athens, Greece. *EPJ Web Conf.* **2018**, *176*, 05025. [CrossRef]
10. Yang, L.; Qiu, J.; Zheng, S.; Xia, Q.; Huang, Q.; Wang, W.; Pan, J. Lidar Measurement of Aerosol, Ozone and Clouds in Beijing. *Proc. SPIE* **2003**, *4893*, 45–51. [CrossRef]
11. Chen, Z.; Zhang, J.; Zhang, T.; Liu, W.; Liu, W. Haze observations by simultaneous lidar and WPS in Beijing before and during APEC. *Sci. China Chem.* **2015**, *58*, 1385–1392. [CrossRef]
12. Seabrook, J.; Whiteway, J. Influence of mountains on Arctic tropospheric ozone. *J. Geophys. Res. Atmos.* **2016**, *121*, 1935–1942. [CrossRef]
13. Steinbrecht, W.; McGee, T.J.; Twigg, L.W.; Claude, H.; Sch¨onenborn, F.; Sumnicht, G.K.; Silbert, D. Intercomparison of stratospheric ozone and temperature profiles during the October 2005 Hohenpeißenberg Ozone Profiling Experiment (HOPE). *Atmos. Meas. Tech.* **2009**, *2*, 125–145. [CrossRef]
14. Sullivan, J.T.; McGee, T.J.; Sumnicht, G.K.; Twigg, L.W.; Hoff, R.M. A mobile differential absorption lidar to measure sub-hourly fluctuation of tropospheric ozone profiles in the Baltimore–Washington, D.C. region. *Atmos. Meas. Tech.* **2014**, *7*, 3529–3548. [CrossRef]
15. Shunxing, H.; Huanling, H.; Yonghua, W.; Jun, Z.; Qi, F.; Yue, G. Atmospheric ozone measured by differential absorption lidar over Hefei. *Proc. SPIE* **2003**, *4893*, 473–479. [CrossRef]
16. Liu, X.; Zhang, Y.; Hu, H.; Tan, K.; Tao, Z.; Shao, S.; Cao, K.; Fang, X.; Yu, S. Mobile lidar for measurements of SO_2 and 03 in the low troposphere. *Proc. SPIE* **2005**, *5832*, 156–163. [CrossRef]
17. Brinksma, E.J.; Swart, D.P.J.; Bergwerff, J.B.; Meijer, Y.J.; Ormel, F.T. RIVM Stratospheric Ozone Lidar at NDSC Station Lauder: Routine Measurements and Validation During the OPAL Campaign. *Adv. Atmos. Remote Sens. Lidar* **1996**, *128*, 529–532. [CrossRef] [PubMed]
18. McDermid, I.S.; Daniel, W.T.; Deslis, A.; White, M.L. Optical systems design for a stratospheric lidar system. *Appl. Opt.* **1995**, *34*, 6201–6210. [CrossRef] [PubMed]

19. Portafaix, T.; Godin-Beekmann, S.; Payen, G.; de Mazière, M.; Langerock, B.; Fernandez, S.; Posny, F.; Cammas, J.P.; Metzger, J.M.; Bencherif, H.; et al. Ozone profiles obtained by DIAL technique at Maïdo Observatory in La Reunion Island: Comparisons with ECC ozone-sondes, ground-based FTIR spectrometer and microwave radiometer measurements. In Proceedings of the 27th International Laser Radar Conference (ILRC 27), New York, NY, USA, 5–10 July 2015; p. 05005. [CrossRef]
20. Baray, J.-L.; Courcoux, Y.; Keckhut, P.; Portafaix, T.; Tulet, P.; Cammas, J.-P.; Hauchecorne, A.; Godin-Beekmann, S.; De Mazière, M.; Hermans, C.; et al. Maïdo observatory: A new high-altitude station facility at Reunion Island (21 S, 55 E) for long-term atmospheric remote sensing and in situ measurements. *Atmos. Meas. Tech.* **2013**, *6*, 2865–2877. [CrossRef]
21. Godin, S.; Bergeret, V.; Bekki, S.; David, C.; Mégie, G. Study of the interannual ozone loss and the permeability of the Antarctic Polar Vortex from long-term aerosol and ozone lidar measurements in Dumont d'Urville (66.4°, 140°S). *J. Geophys. Res.* **2001**, *106*, 1311–1330. [CrossRef]
22. Gaudel, A.; Ancellet, G.; Godin-Beekmann, S. Analysis of 20 years of tropospheric ozone vertical profiles by lidar and ECC at Observatoire de Haute Provence (OHP) at 44 N, 6.7 E. *Atmos. Environ.* **2015**, *113*, 78–89. [CrossRef]
23. Park, C.B.; Nakane, H.; Sugimoto, N.; Matsui, I.; Sasano, Y.; Fujinuma, Y.; Ikeuchi, I.; Kurokawa, J.-I.; Furuhashi, N. Algorithm improvement and validation of National Institute for Environmental Studies ozone differential absorption lidar at the Tsukuba Network for Detection of Stratospheric Change complementary station. *Appl. Opt.* **2006**, *45*, 3561–3576. [CrossRef]
24. Nakazato, M.; Nagai, T.; Sakai, T.; Hirose, Y. Tropospheric ozone differential-absorption lidar using stimulated Raman scattering in carbon dioxide. *Appl. Opt.* **2007**, *46*, 2269–2279. [CrossRef] [PubMed]
25. Veselovskii, I.; Barchunov, B. Excimer-laser-based lidar for tropospheric ozone monitoring. *Appl. Phys.* **1999**, *68*, 1131–1137. [CrossRef]
26. McDermid, I.S.; Godin, S.M.; Lindquist, L.O. Ground-based laser DIAL system for long-term measurements of stratospheric ozone. *Appl. Opt.* **1990**, *29*, 3603–3612. [CrossRef] [PubMed]
27. McDermid, I.S.; Beyerle, G.; Haner, D.A.; Leblanc, T. Redesign and improved performance of the tropospheric ozone lidar at the Jet Propulsion Laboratory Table Mountain Facility. *Appl. Opt.* **2002**, *41*, 7550–7555. [CrossRef] [PubMed]
28. Dolgii, S.I.; Nevzorov, A.A.; Nevzorov, A.V.; Romanovskii, O.A.; Makeev, A.P.; Kharchenko, O.V. Lidar Complex for Measurement of Vertical Ozone Distribution in the Upper Troposphere–Stratosphere. *Atmos. Ocean. Opt.* **2018**, *31*, 702–708. [CrossRef]
29. Pavlov, A.N.; Stolyarchuk, S.Y.; Shmirko, K.A.; Bukin, O.A. Lidar Measurements of Variability of the Vertical Ozone Distribution Caused by the Stratosphere–Troposphere Exchange in the Far East Region. *Atmos. Ocean. Opt.* **2013**, *26*, 126–134. [CrossRef]
30. Fang, X.; Li, T.; Ban, C.; Wu, Z.; Li, J.; Li, F.; Cen, Y.; Tian, B. A mobile differential absorption lidar for simultaneous observations of tropospheric and stratospheric ozone over Tibet. *Opt. Express.* **2019**, *27*, 4126–4139. [CrossRef] [PubMed]
31. Gorshelev, V.; Serdyuchenko, A.; Weber, M.; Chehade, W.; Burrows, J.P. High spectral resolution ozone absorption cross-sections—Part 1: Measurements, data analysis and comparison with previous measurements around 293 K. *Atmos. Meas. Tech.* **2014**, *7*, 609–624. [CrossRef]
32. Serdyuchenko, A.; Gorshelev, V.; Weber, M.; Chehade, W.; Burrows, J.P. High spectral resolution ozone absorption cross-sections—Part 2: Temperature dependence. *Atmos. Meas. Tech.* **2014**, *7*, 625–636. [CrossRef]
33. Dolgii, S.; Nevzorov, A.A.; Nevzorov, A.V.; Romanovskii, O.A.; Kharchenko, O.V. Intercomparison of Ozone Vertical Profile Measurements by Differential Absorption Lidar and 5 IASI/MetOp Satellite in the Upper Troposphere6 Lower Stratosphere. *Remote Sens.* **2017**, *9*, 447. [CrossRef]
34. Clerbaux, C.; Boynard, A.; Clarisse, L.; George, M.; Hadji-Lazaro, J.; Herbin, H.; Hurtmans, D.; Pommier, M.; Razavi, A.; Turquety, S.; et al. Monitoring of atmospheric composition using the thermal infrared IASI/MetOp sounder. *Atmos. Chem. Phys.* **2009**, *9*, 6041–6054. [CrossRef]
35. El'nikov, A.V.; Marichev, V.N.; Shelevoi, K.D.; Shelefontyuk, D.I. Laser Radar for Sensing Vertical Stratification of Atmospheric Aerosol. *Atmos. Ocean. Opt.* **1988**, *1*, 117–123.
36. NASA (National Aeronautics and Space Administration). MLS Ozone Data. Available online: https://avdc.gsfc.nasa.gov/pub/data/satellite/Aura/MLS/ (accessed on 5 May 2024).
37. Matvienko, G.G.; Belan, B.D.; Panchenko, M.V.; Romanovskii, O.A.; Sakerin, S.M.; Kabanov, D.M.; Turchinovich, S.A.; Turchinovich, Y.S.; Eremina, T.A.; Kozlov, V.S.; et al. Complex experiment on studying the microphysical, chemical, and optical properties of aerosol particles and estimating the contribution of atmospheric aerosol-to-earth radiation budget. *Atmos. Meas. Tech.* **2015**, *8*, 4507–4520. [CrossRef]